From Mott insulator to band insulator: A dynamical mean-field theory study

Andreas Fuhrmann, David Heilmann, and Hartmut Monien
Physikalisches Institut, Universität Bonn, Nußallee 12, 53115 Bonn, Germany
(Received 17 October 2005; revised manuscript received 7 April 2006; published 28 June 2006)

The question if a Mott insulator and a band insulator are fundamentally different has been the matter of intensive research recently. Here we consider a simple model which allows by tuning one parameter to go continuously from a Mott insulator to band insulator. The model consists of two Hubbard systems connected by single particle hopping. The Hubbard Hamiltonian is solved by the dynamical mean-field theory using Quantum Monte Carlo to solve the resulting quantum impurity problem. The quasiparticle spectral function is calculated. Here we focus on the optical conductivity and in particular on the Drude weight which can be experimentally measured. From our calculation we conclude that there is a continuous crossover from the band insulator to the Mott insulator phase at finite temperature.

DOI: 10.1103/PhysRevB.73.245118 PACS number(s): 71.10.Fd, 71.27.+a, 71.30.+h, 72.15.−v

I. INTRODUCTION

Recently the question whether a Mott insulator and a band insulator are fundamentally different has been raised.[1–8] To study this question, we consider the simplest model which allows one, by tuning one parameter, to obtain a Mott insulator as well as a band insulator phase. The model consists of two Hubbard systems with strong on-site Coulomb repulsion which are connected by single particle hopping. This model can be viewed as a model for two planes of strongly correlated electrons on a square lattice with on-site interaction and hopping connecting corresponding sites of the two planes. At half filling with no interaction the metal-to-band insulator transition is driven by increasing the hopping between the two subsystems, i.e., the splitting of the bonding and antibonding bands produces a gap. In the case of no hopping between the planes, a Mott transition is driven by increasing the on-site Coulomb repulsion, which localizes the electrons by suppressing the hopping between different sites. The overall scale of the problem is set by the hopping matrix element t within the plane (which we set to unity) and the parameter differentiating between the Mott and band insulator is the ratio of the hopping matrix element between the planes, $t_\perp$, and the on-site Coulomb repulsion U. The approximation used in this work consists of letting the coordination number of the sites in each plane (4) to go to infinity. This model has been studied with dynamical mean-field theory (DMFT) approximation using iterated perturbation theory (IPT) at zero temperature.[9,10] We study this model at finite temperature using Quantum Monte Carlo (QMC)[11,12] as impurity solver. Also, first successful attempts to apply a more demanding continuous-time QMC algorithm to a simplified two-impurity problem already exist.[13] Here, the focus is on the nature of the transition from the Mott insulator to the band insulator phase. We calculate the optical conductivity for direct comparison with experimental data. For other theoretical studies of low-dimensional coupled strongly correlated systems see, e.g., Essler and Tsvelik,[1] Potthoff and Nolting,[14,15] Biermann *et al.*,[16,17] Koga *et al.*[18]

The rest of this paper is organized as follows: First, we introduce the Hamiltonian and present the solution method using DMFT and the Quantum Monte Carlo algorithm. We use these methods to determine the metal-to-insulator transition and calculate the phase diagram of the model at finite temperature. Then we consider and analyze the numerical results, in particular the analytic continuation of the imaginary-time QMC data. We present detailed results for the single-particle spectral function and the optical conductivity close to the transition and analyze the behavior of these properties close to the transition. Finally, we state our conclusions.

II. FORMALISM

A. The model and solution method

The two-plane Hubbard model with interplane hopping $t_\perp$ is described by the Hamiltonian

$$H = -\frac{1}{\sqrt{z}}\sum_{\langle i,j\rangle\sigma\alpha} c^+_{i\sigma\alpha}c_{j\sigma\alpha} - t_\perp\sum_{i\sigma\alpha} c^+_{i\sigma\alpha}c_{i\sigma,1-\alpha} + U\sum_{i\alpha} n_{i\uparrow\alpha}n_{i\downarrow\alpha} \tag{1}$$

with $c_{i\sigma\alpha}$ denoting the annihilation operator for an electron/hole with spin component σ on site i of the plane $\alpha=0,1$, and $n_{i\sigma\alpha}=c^+_{i\sigma\alpha}c_{i\sigma\alpha}$. This means electrons can move inside the planes as well as between corresponding sites on the two planes. z denotes the coordination number of the lattice ($z=4$ for two dimensions), ensuring a constant bandwidth as the coordination number is taken toward infinity.

Using dynamical mean-field theory,[19–21] the two-plane system is reduced to two impurities self-consistently embedded in a bath: In order to calculate on-site (local) properties of the sites $(i,\alpha)=(i,0),(i,1)$ (site i of each of the planes), the self-energy $\Sigma_{\alpha\alpha'}(\omega,\mathbf{k})$ is replaced by the local self-energy $\Sigma_{\alpha\alpha'}(\omega,0)$, leading to a two-impurity ($i=0$, $\alpha=0,1$) problem given by the "effective" action

$$S[(c^+_{0\sigma\alpha},c_{0\sigma\alpha})_{\sigma\alpha}] = \int d\tau d\tau' \sum_{\sigma\alpha\alpha'} c^+_{0\sigma\alpha}(\tau)\mathcal{G}_{\alpha\alpha'}(\tau,\tau')^{-1}c_{0\sigma\alpha'}(\tau') + U\int d\tau\sum_{\alpha} n_{0\alpha\uparrow}(\tau)n_{0\alpha\downarrow}(\tau). \tag{2a}$$

The Weiss field $\mathcal{G}$ describes the dynamics of the site $i=0$

without the interaction plus the rest of the lattice. $\mathcal{G}$ is a 2×2 matrix; since the system is symmetric under exchange of the planes, we use $\mathcal{G}_{00}=\mathcal{G}_{11}=:\mathcal{G}_0$, $\mathcal{G}_{01}=\mathcal{G}_{10}=:\mathcal{G}_1$; the properties of the system can be described by the symmetric/antisymmetric (bonding/antibonding) combinations of the two planes. This impurity problem is defined by the self-consistency equation

$$\mathcal{G}_{\mathrm{S/A}}(i\omega_n)^{-1}=\Sigma_{\mathrm{S/A}}(i\omega_n)+\tilde{D}(i\omega_n+\mu\mp t_\perp-\Sigma_{\mathrm{S/A}}(i\omega_n))^{-1}, \tag{2b}$$

where $\tilde{D}(\zeta)=\int d\varepsilon D(\varepsilon)(\zeta-\varepsilon)^{-1}$, D being the density of states (DOS) for a free ($U=0$) single-plane system, $\mathcal{G}_{\mathrm{S/A}}=\mathcal{G}_0\pm\mathcal{G}_1$, $\Sigma_{\mathrm{S/A}}=\Sigma_0\pm\Sigma_1$, and Σ is the self-energy for the impurity problem, which can be calculated from the effective impurity action via the impurity Green's function (the mean-field approximation for the on-site lattice Green's function). The self-consistency equation can be derived exactly following the lines given in the work by Georges *et al.*[21]

Moreover, D is the only place where the detailed lattice structure enters the calculations, so the results are essentially independent of those details.

The DMFT equations are usually solved using an iteration algorithm consisting of two parts: By solving an impurity-like problem (2a), the on-site Green's function is determined, then, using the DMFT self-consistency equation (2b), a new impurity problem is defined. This is repeated until convergence has apparently been reached.

We solve the two impurity problem using the Quantum Monte Carlo algorithm developed by Hirsch and Fye.[12] In order to use the Monte Carlo algorithm with the DMFT effective action which is nonlocal with respect to imaginary time τ, the action S has to be rewritten[21] using a lattice Hamiltonian consisting of auxiliary "bath" orbitals, replacing the bath Green's function $\mathcal{G}$.

For initialization, we use a guess for the Weiss fields, $\mathcal{G}_0^{\mathrm{guess}}(i\omega_n)$ (diagonal, i.e., connecting one site to itself) and $\mathcal{G}_1^{\mathrm{guess}}(i\omega_n)$ (off-diagonal, i.e., connecting one site to the corresponding site on the other plane), determining the Green's function of the lattice. Using the QMC algorithm, the local imaginary-time Green's functions $G_0(\tau)$ and $G_1(\tau)$ are calculated, G_0 being the on-site Green's function, whereas G_1 is again connecting two corresponding sites on different planes. Use of the Dyson equation then yields the self-energies $\Sigma_0(i\omega_n)$ and $\Sigma_1(i\omega_n)$.

Now, in order to use the self-consistency equation, we switch to the symmetric/antisymmetric (S/A) combinations of the two planes, so the self-energy, the Green's function, and the Weiss field become diagonal 2×2 matrices. Since the kinetic energy is then diagonal as well, the free Green's functions are the Hilbert transforms of the density of states for the symmetric/antisymmetric combinations of the real-space planes without interaction:

$$G^0_{\mathrm{S/A}}(i\omega_n)=\tilde{D}(i\omega_n+\mu\mp t_\perp). \tag{3}$$

Therefore the self-energy can be easily calculated using

$$\Sigma_{\mathrm{S/A}}(i\omega_n)=\tilde{D}(i\omega_n+\mu\mp t_\perp)^{-1}-G_{\mathrm{S/A}}(i\omega_n)^{-1}, \tag{4}$$

where $G_{\mathrm{S/A}}=G_0\pm G_1$. Now we can calculate the new Weiss fields for the next iteration using the self-consistency equation (2b).

B. Optical conductivity

Using the electron spectral densities $A_{\mathrm{S/A}}(\omega)$, we calculate the electron self-energy at real frequencies, $\Sigma_{\mathrm{S/A}}(\omega)$. The spectral function for a nonvanishing momentum is then given to be $A_\varepsilon^{\mathrm{S/A}}(\omega)=-\mathrm{Im}\,G_{\mathrm{S/A}}(\omega+i0,\varepsilon)/\pi=-\mathrm{Im}(1/(\omega+i0\mp t_\perp-\varepsilon-\Sigma_{\mathrm{S/A}}(\omega)))/\pi$, where ε is the free-particle kinetic energy.

The optical conductivity is, up to a constant, defined by

$$\sigma(\nu)=\frac{i\sigma_0}{\nu+i\cdot 0}G_{jj}(\nu+i\cdot 0), \tag{5}$$

where G_{jj} denotes the current-current correlation function. As a function of the bosonic Matsubara frequencies ν_m, in DMFT for a hypercubic lattice, it is[21]

$$G_{jj}(i\nu_m)=\sum_{\alpha=\mathrm{S,A}}\int_{-\infty}^{\infty}d\varepsilon D(\varepsilon)\times\frac{1}{\beta}\sum_{n=-\infty}^{\infty}G_\alpha(i\omega_n,\varepsilon)G_\alpha(i\omega_n+i\nu_m,\varepsilon). \tag{6}$$

After continuation to real frequencies ω, the real (nondissipative) part of the optical conductivity is, up to the constant[22] σ_0,

$$\mathrm{Re}\,\sigma(\omega)=\sigma_0\int d\varepsilon D(\varepsilon)\sum_{\alpha=\mathrm{S,A}}\int d\omega'\times A_\varepsilon^\alpha(\omega')A_\varepsilon^\alpha(\omega+\omega')\frac{f(\omega')-f(\omega+\omega')}{\omega}, \tag{7}$$

f denoting the Fermi function, $f(\omega)=1/(\exp(\beta\omega)+1)$, where β denotes the inverse temperature. Finally, the weight of the Drude peak was determined by fitting a Lorentz curve to the central peak (the first five data points, corresponding to $\omega<2/\beta$).

The reason for the summation over symmetric and antisymmetric planes in Eqs. (6) and (7) is the following: since the optical conductivity is defined as a long-wavelength limit, the momentum transferred by the optical conductivity has to vanish, viz. the in-plane component as well as the component perpendicular to the planes. The perpendicular component can assume just two values, 0 and π/(plane distance), corresponding to symmetric and antisymmetric orbitals, respectively. Therefore, the optical conductivity at vanishing (also perpendicular) momentum is given by the product of Green's functions both symmetric or both antisymmetric.

In the limit of high dimension, interband transitions do not contribute to the optical conductivity, as they may only arise from interaction vertices. However, in that limit, the interaction only contributes to the optical conductivity via

self-energy insertions in the single-particle Green's function,[21] quite regardless of the detailed band-index structure of the interaction vertex.

The replacement of the Gaussian free DOS of the hypercubic lattice by a semicircular one (which is the exact DOS for an infinite-coordination Bethe lattice) is an ad-hoc approximation, which may be justified by the low weight of the Gaussian tails and their unphysicality. However, Eq. (6) was derived for a hypercubic lattice with Gaussian DOS, so, although we assume our results to be realistic, they still are based on a substantial approximation. For a detailed discussion of possible transport properties on a Bethe lattice, please refer to Blümer and van Dongen.[23,24]

III. NUMERICAL RESULTS

A. Single particle density of states

We consider the half-filled model ($n=1$) at a temperature $T=0.025=1/\beta$, using $L=100$ time slices of $\Delta\tau=\beta/L=0.4$. As the density of states of the free ($U=0$) uncoupled ($t_\perp=0$) lattice, we use a semicircular $D(\varepsilon)=\sqrt{4-\varepsilon^2}/(2\pi)$, which becomes exact for electrons on a Bethe lattice.[21] This is more convenient than a Gaussian DOS for a hypercubic lattice, because the extended unphysical tails of the Gauss distribution render it impossible to clearly define the metal-to-band insulator transition.

From the imaginary-time Green's functions produced by the QMC algorithm, the corresponding spectral densities for the symmetric/antisymmetric planes are extracted using the maximum-entropy method.[25,26] We use a default model consisting of normalized semi-ellipses of half-width $U/2+2$ centered at $\mp t_\perp$ for the symmetric and antisymmetric plane, respectively, plus a small flat "background" in order to keep the possibility to extract features outside this area. Alternatively, a flat and a Gaussian default model were used; however, those produce unphysically large high-frequency tails in the spectral density and, as well, artificial humps at $\omega=0$ even in the noninteracting case. Figure 1 shows the density of states of the uncoupled system ($t_\perp=0$) at $U=1$, 2, 3, 4.5, 4.75, and 6. The DOS at $U=4.5$ has a three-peak shape characteristic for the metallic state close to the Mott transition. The optical conductivity and the Drude weight yield a transition value $U\approx 4.7$ (Fig. 4). As the iteration was initialized using an "insulating" Green's function, the transition marks the lower-U end of the coexistence region. The spectral density at $U=4.75$ represents the insulating state just after the vanishing of the quasiparticle peak. The DOS at $U=6$ displays the lower and upper Hubbard bands at $-U/2$ and $+U/2$, respectively.

At $U=0$, the metal-to-band insulator transition was found at $t_\perp=2.0$ (see also the phase diagram, Fig. 7). This is the point where the overlap of the spectral densities for the symmetric and the antisymmetric planes vanishes. The spectral densities for the metallic and the band insulating phases are given in Fig. 2. As can be seen, the spectral densities for the symmetric/antisymmetric plane are shifted from their $t_\perp=0$ position by exactly $\mp t_\perp$. The symmetric DOS at $t_\perp=2$ corresponds to the state right at the band transition. The error bars are of the order of magnitude of the linewidth.

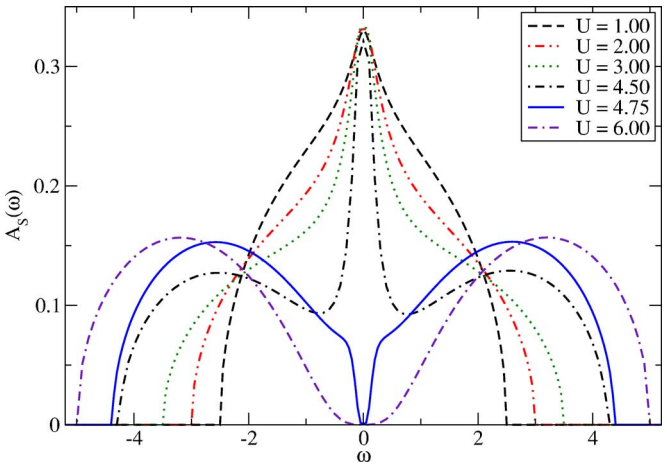

FIG. 1. (Color online) Mott transition. Spectral densities of the uncoupled ($t_\perp=0$) two-plane Hubbard model. The DOS correspond to the metallic state ($U=1,2,3,4.5$), and to the insulating state ($U=4.75,6$). The DOS at $U=4.75$ corresponds to the insulating state slightly above the Mott transition. The iteration was initialized using an insulating Green's function.

For finite U, on increasing $t_\perp$, for the symmetric plane, the weight of the upper Hubbard band is reduced, whereas the lower one increases, until, at $t_\perp>2$, the upper Hubbard band has completely vanished. For the antisymmetric plane, the upper band is increased at the expense of the lower one. For intermediate values, this effect can be clearly seen from Fig. 3.

Our results are compatible with earlier results for the single-plane model found by different methods like QMC or IPT[21] or NRG[27] (the upper boundary of the coexistence region is slightly higher in our case, due to very large time slices). As discussed in the following, our results are also compatible to the quantities calculated for a two-plane model by Moeller *et al.*,[10] although those are zero-temperature data.

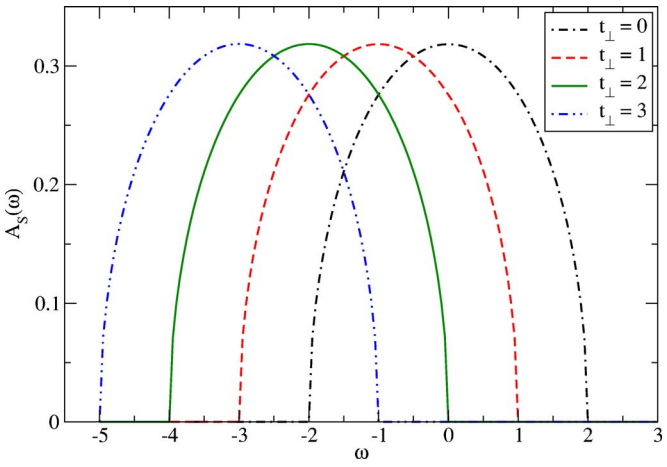

FIG. 2. (Color online) Band transition. Reconstructed spectral densities of the symmetric plane of the free two-plane Hubbard model at $U=0$, $t_\perp=0,1,2,3$. The antisymmetric DOS is $A_A(\omega)=A_S(-\omega)$. A_S and A_A do not overlap in the band insulating state, the band transition occurs at $t_\perp=2$.

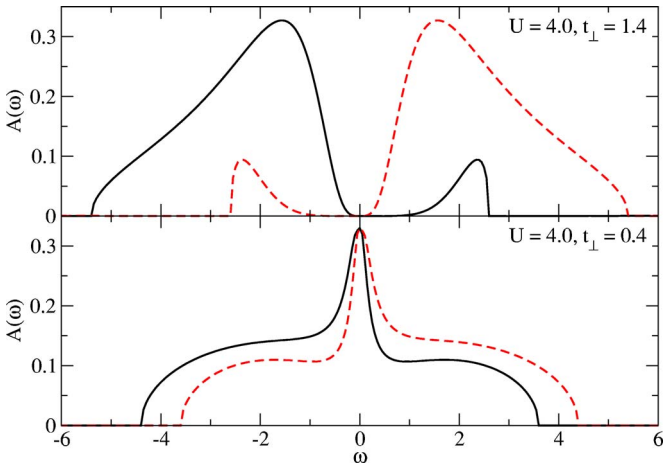

FIG. 3. (Color online) Reconstructed symmetric (solid line) and antisymmetric (broken line) spectral densities of the two-plane Hubbard model at $U=4$ and $t_\perp=0.4$, 1.4 using $L=100$ time slices. The changes of the Hubbard bands due to $t_\perp$ can be clearly seen. Due to particle-hole symmetry of the two-plane system at half filling, the overall spectral density is symmetric.

B. Optical conductivity

At first, we consider the optical conductivity of the uncoupled system ($t_\perp=0$). Using the spectral densities obtained by maximum-entropy, we found the optical conductivity for different values of U (Fig. 4) using Eq. (7). Our results are compatible with the single-plane data in Pruschke *et al.*[22]

The quasiparticle contribution to conduction is given by the weight of the Drude peak located at $\omega=0$, thus, an insulating system has vanishing Drude weight. With increasing interaction parameter U, the Drude peak decreases for all values of $t_\perp$. As well, the growth of the incoherent peak at $\omega\approx U$ is clearly visible. In the inset, the Drude weight is shown as a function of U. Clearly, the system becomes a

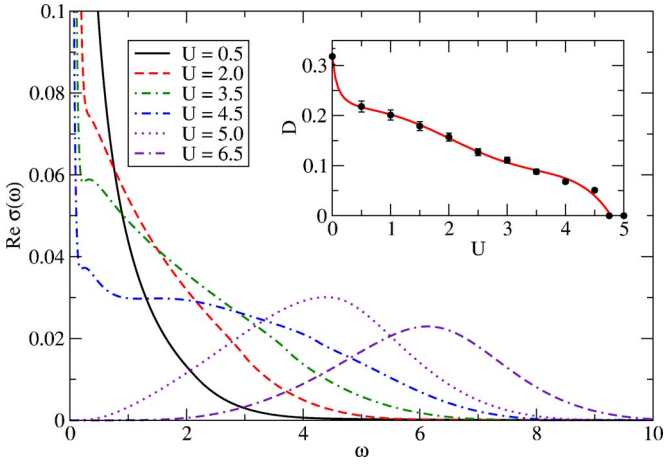

FIG. 4. (Color online) The evolution of the optical conductivity as a function ω at different U, $t_\perp=0$. Inset: formation of the Drude weight with increasing U. As can be seen, the Drude weight vanishes at $U\approx4.7$. Because the iteration was initialized using an "insulating" Green's function, this is the lower end of the coexistence region.

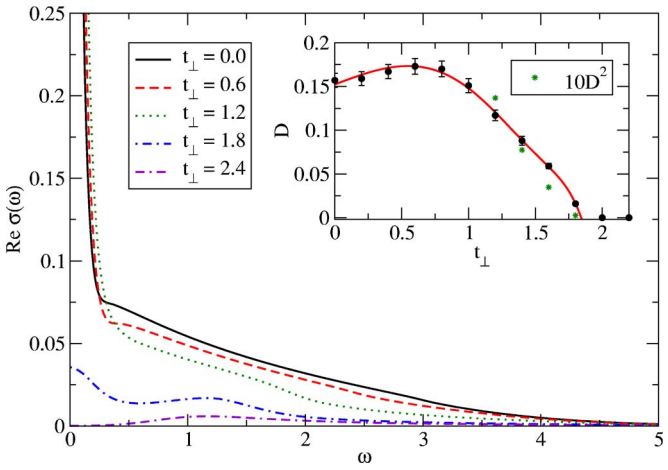

FIG. 5. (Color online) The evolution of the optical conductivity as a function ω at different $t_\perp$, $U=2$. Inset: formation of the Drude weight with increasing $t_\perp$. As can be seen, the Drude weight vanishes at $t_\perp\approx1.8$, where a metal-to-insulator transition takes place.

Mott insulator at $U\approx4.7$, if the iteration is initialized with an "insulating" Green's function. Figure 5 depicts the optical conductivity for different $t_\perp$ at $U=2$, again consisting of the Drude peak of different weights and an "incoherent" part which consists of two peaks, one of them located at $\omega\approx U$, the other one, present only in the metallic phase, located at $\omega\approx U/2$. However, the latter one is usually smeared too strongly to be seen clearly,[22] only for low values of $t_\perp$, some traces of this peak might be recognized. With increasing $t_\perp$, the Drude peak vanishes at $t_\perp\approx1.8$ for $U=2$, indicating the transition to a predominantly band insulating state. The transition value was found by linear extrapolation of the squared Drude weight (see the inset of Fig. 5).

C. Phase diagram

In Fig. 6, the Drude weights for the different values of $(t_\perp, U)$ are shown. In order to find the metal-to-insulator transitions we used a linear interpolation of the quadratic value of the Drude weight, obtaining the phase diagram given in Fig. 7. The different regions of the phase diagram could be clearly located: as expected, there is a metallic state for low U and low $t_\perp$, which is bounded by a metal-to-band insulator transition at $t_\perp=2$. For high U, the system is in a

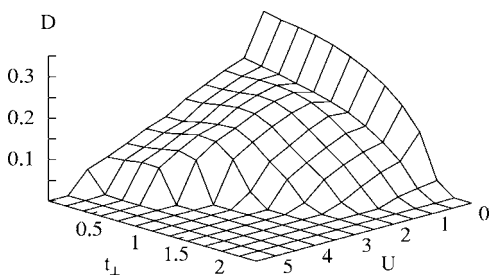

FIG. 6. Drude weight D at temperature $T=0.025$, the iteration was initialized with an "insulating" Green's function. The region $D\neq0$ can thus be identified as the low-U, low-$t_\perp$ region, as also depicted in Fig. 7.

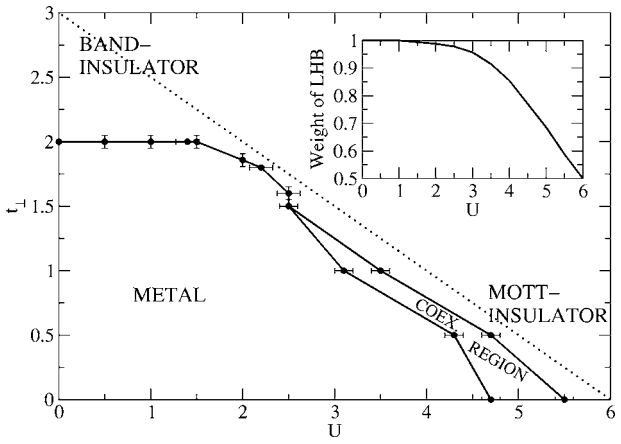

FIG. 7. Finite-temperature ($T=0.025$) phase diagram. The lines are just a guide to the eye. Inset: the evolution of the weight of the lower Hubbard band of the symmetric plane on the dotted line. By comparing to Fig. 6, the metallic region is recognized as the region with nonvanishing Drude weight.

Mott insulating state; the metallic and insulating solutions are both locally stable within a coexistence region. As discussed in the following, no clear separation between the Mott and the band insulating states was found.

In order to get some impression of the transition between the band insulating and the Mott insulating phase, we calculated the weight of the lower Hubbard band (LHB) of the symmetric plane which is defined as $\int_{-\infty}^{0} d\omega A_S(\omega)$, at the points given by the dotted line in Fig. 7. Some of the spectral density functions can be seen in Fig. 8. The evolution of the LHB weight along the dotted line is shown in the inset in Fig. 7. For half filling, the weight of the LHB for a purely band insulating phase is unity, for a purely Mott insulating phase, it is close to 0.5. As can be seen the weight of the LHB does not show either some distinct kink or vanish from

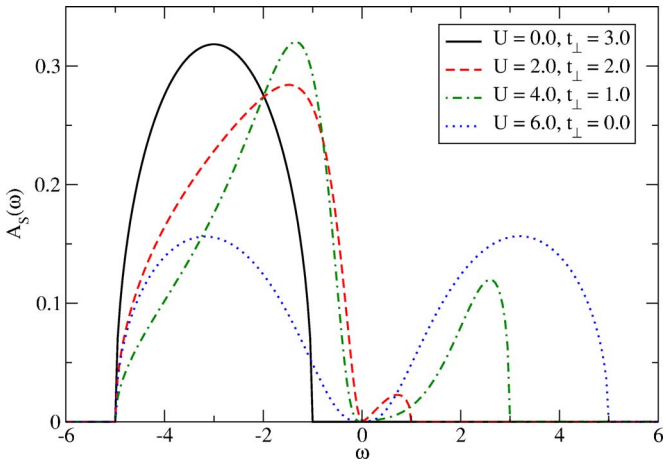

FIG. 8. (Color online) Selection of reconstructed symmetric spectral densities on the dotted line in Fig. 7, at temperature $T=0.025$. A purely Mott insulating state is characterized by a spectral density of the symmetric or antisymmetric plane, respectively, divided by half into a lower and an upper Hubbard band, whereas a purely band insulating state means the symmetric band is entirely located below $\omega=0$, and the antisymmetric band entirely above.

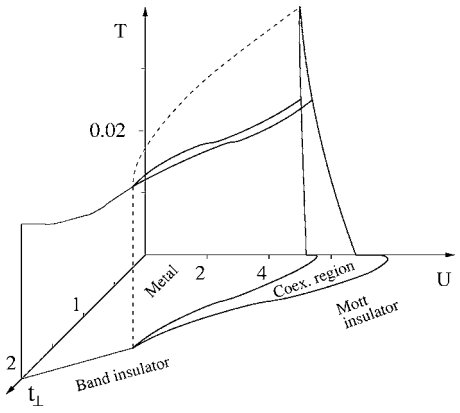

FIG. 9. Three-dimensional phase diagram of the two-plane Hubbard model, composed of the data in Moeller *et al.* Ref. 10 ($T=0$), Georges *et al.* Ref. 21 ($t_\perp=0$), and this work. The dashed line indicates the shape of the coexistence region suggested by the data, which are indicated by the full lines; thin lines indicate the metal-to-insulator transitions.

a well-defined point. Thus, this quantity does not yield any evidence for a phase transition between the Mott-Hubbard and the band insulating phase.

We find a phase diagram which is clearly compatible to the zero-temperature phase diagram in Moeller *et al.*,[10] keeping in mind that $U_{\text{Moeller}}=U/2$ and $t_{ab\text{Moeller}}=t_\perp/2$. However, some differences ought to be noticed: the coexistence region is found at a lower U value due to the finite temperature (see, for comparison, the phase diagram in Georges *et al.*,[21] where the same scale of U is used as by Moeller *et al.*[10]); the coexistence region has become smaller as well. A coexistence region thus clearly exists at a temperature of $T=0.025$; in contrast, at $T=0.05$, no coexistence region was found anymore. This behavior suggests that the critical temperature of the Mott transition decreases as $t_\perp$ is increasing, see the sketch in Fig. 9.

The other clear difference is the slope of the transition line at low interaction U, close to the band transition. We find, for low U, the transition line to be at almost constant $t_\perp$, whereas Moeller *et al.* find a clear dependence on $t_\perp$. We assume this is due to the temperature: as a finite temperature always smoothens a metal-to-band insulator transition, a small interaction driving the system to an insulating state can be compensated by thermal fluctuations.

The re-entrance behavior seen in the IPT[10] cannot be resolved accurately in our calculation. The general shape of the phase boundary however suggests that a re-entrance behavior does not exist at the temperature considered. To resolve this issue definitely, lower temperatures have to be considered which are inaccessible to the Hirsch-Fye algorithm for the large-U case.

The comparatively[21] high upper bound of the coexistence region may be due to the non-negligible Trotter error in this region. The insulating solution will be much less sensitive to an increase in the $(U\Delta\tau)^2$ term neglected by the Trotter decomposition of the path integral than the metallic solution, which is why the upper bound shifts due to the truncation error, but not so much the lower bound, which is also at a lower U value, so the second-order U term neglected by the time discretization is smaller.

IV. SUMMARY

In summary, we have calculated the spectral densities, the optical conductivities, and the Drude weights of a two-plane Hubbard model at low temperature for different values of the interplane coupling. We have located the different metal-to-insulator transitions; however, no clear transition between the Mott insulating phase and the band insulating phase could be found; as well, the corresponding spectral weights show a continuous behavior. This observation is consistent with the assumption that there exists only a crossover between those two insulating phases, but no clear phase transition. The phase diagram is slightly different from the one found in Moeller *et al.*,[10] which comes as no surprise as we are considering finite temperature shifting transition values and decreasing the coexistence region.

We have discussed in detail spectral properties like, e.g., the optical conductivity, which is of some use to experimentalists. Also, the use of a Quantum Monte Carlo method means a serious technical improvement with respect to earlier studies, as it is a numerically exact method without the use of uncontrolled approximations.

Even though the use of a Quantum MC algorithm[12] means a technical advantage, the behavior of the system for very low temperatures could not be considered in this work. We plan to investigate lower temperatures using a very recently developed continuous-time Quantum Monte Carlo algorithm,[28,29] yielding the phase diagram at much lower temperatures and clarifying the evolution toward zero temperature.

ACKNOWLEDGMENTS

We are thankful for the hospitality of the Aspen Centre for Physics (H.M.), Rutgers University, and Columbia University. Fruitful discussions with A. Georges, M. Imada, G. Kotliar, W. Krauth, A. I. Lichtenstein, A. J. Millis, and O. Parcollet are gratefully acknowledged. This work was supported by Grant Nos. SFB 608 and SPP 1073 of the Deutsche Forschungsgemeinschaft and a grant by the DAAD (German Academic Exchange service) (A.F.).

[1] F. H. L. Essler and A. M. Tsvelik, Phys. Rev. B **65**, 115117 (2002).
[2] I. Dzyaloshinskii, Phys. Rev. B **68**, 085113 (2003).
[3] F. H. L. Essler and A. M. Tsvelik, Phys. Rev. B **71**, 195116 (2005).
[4] R. M. Konik, T. M. Rice, and A. M. Tvelik, cond-mat/0511268 (unpublished).
[5] C. Berthod, T. Giamarchi, S. Biermann, and A. Georges, cond-mat/0602304 (unpublished).
[6] A. Rosch, cond-mat/0602656 (unpublished).
[7] T. D. Stanescu, P. W. Phillips, and T.-P. Choy, cond-mat/0602280 (unpublished).
[8] K.-Y. Yang, T. M. Rice, and F.-C. Zhang, cond-mat/0602164 (unpublished).
[9] H. Monien, N. Elstner, and A. J. Millis, cond-mat/9707051 (unpublished).
[10] G. Moeller, V. Dobrosavljević, and A. E. Ruckenstein, Phys. Rev. B **59**, 6846 (1999).
[11] J. E. Hirsch, Phys. Rev. B **28**, R4059 (1983).
[12] J. E. Hirsch and R. M. Fye, Phys. Rev. Lett. **56**, 2521 (1986).
[13] V. V. Savkin, A. N. Rubtsov, M. I. Katsnelson, and A. I. Lichtenstein, Phys. Rev. Lett. **94**, 026402 (2005).
[14] M. Potthoff and W. Nolting, Phys. Rev. B **59**, 2549 (1999).
[15] M. Potthoff and W. Nolting, Eur. Phys. J. B **8**, 555 (1999).
[16] S. Biermann, A. Georges, A. Lichtenstein, and T. Giamarchi, Phys. Rev. Lett. **87**, 276405 (2001).
[17] S. Biermann, A. Georges, T. Giamarchi, and A. Lichtenstein, cond-mat/0201542 (unpublished).
[18] A. Koga, K. Inaba, and N. Kawakami, Prog. Theor. Phys. Suppl. **160**, 253 (2005).
[19] W. Metzner, Ph.D. thesis, RWTH Aachen, 1989.
[20] E. Müller-Hartmann, Z. Phys. B: Condens. Matter **74**, 506 (1989).
[21] A. Georges, G. Kotliar, W. Krauth, and M. J. Rozenberg, Rev. Mod. Phys. **68**, 13 (1996).
[22] T. Pruschke, D. L. Cox, and M. Jarrell, Phys. Rev. B **47**, 3553 (1992).
[23] N. Blümer and P. G. J. van Dongen, in *Concepts in Electron Correlation*, edited by A. C. Hewson and V. Zlatic (Kluwer, Dordrecht, 2003), NATO Science Series, ISBN 1-4020-1419-8.
[24] N. Blümer and P. G. J. van Dongen, cond-mat/0303204 (unpublished).
[25] W. von der Linden, Appl. Phys. A: Mater. Sci. Process. **60**, 155 (1995).
[26] M. Jarrell and J. E. Gubernatis, Phys. Rep. **269**, 133 (1996).
[27] R. Bulla, T. A. Costi, and D. Vollhardt, Phys. Rev. B **64**, 045103 (2001).
[28] A. I. Lichtenstein and A. N. Rubtsov, JETP Lett. **80**, 61 (2004).
[29] A. N. Rubtsov, V. V. Savkin, and A. I. Lichtenstein, Phys. Rev. B **72**, 035122 (2005).